CellPress

Cancer Cell
Article

Tumor Vessel Normalization by Chloroquine Independent of Autophagy

Hannelore Maes,[1,15] Anna Kuchnio,[2,3,15] Aleksandar Peric,[4] Stijn Moens,[2,3] Kris Nys,[1] Katrien De Bock,[2,3] Annelies Quaegebeur,[2,3] Sandra Schoors,[2,3] Maria Georgiadou,[2,3] Jasper Wouters,[5,6] Stefan Vinckier,[2,3] Hugo Vankelecom,[6] Marjan Garmyn,[7] Anne-Clémence Vion,[8] Freddy Radtke,[9,10] Chantal Boulanger,[8] Holger Gerhardt,[11,12,13] Elisabetta Dejana,[14] Mieke Dewerchin,[2,3] Bart Ghesquière,[2,3] Wim Annaert,[4] Patrizia Agostinis,[1,*] and Peter Carmeliet[2,3]

[1]Department Cellular and Molecular Medicine, Laboratory of Cell Death and Therapy, KU Leuven, B-3000 Leuven, Belgium
[2]Department of Oncology, Laboratory of Angiogenesis and Neurovascular Link, KU Leuven, B-3000 Leuven, Belgium
[3]Vesalius Research Center, Laboratory of Angiogenesis and Neurovascular Link, VIB, B-3000 Leuven, Belgium
[4]Department of Human Genetics and VIB-Center for the Biology of Disease, Laboratory for Membrane Trafficking, B-3000 Leuven, Leuven 3000, Belgium
[5]Department of Imaging & Pathology, Translational Cell and Tissue Research, KU Leuven, B-3000 Leuven, Belgium
[6]Department of Development and Regeneration, Embryo and Stem Cells Unit, KU Leuven, B-3000 Leuven, Belgium
[7]Department of Oncology, Laboratory Dermatology, KU Leuven, B-3000 Leuven, Belgium
[8]Cardiovascular Research Center, INSERM UMR-970, Paris Cedex 15, France
[9]Ecole Polytechnique Fédérale de Lausanne, School of Life Science, 1015 Lausanne, Switzerland
[10]Swiss Institute for Experimental Cancer Research, 1015 Lausanne, Switzerland
[11]Vascular Biology Laboratory, London Research Institute, Cancer Research UK, London WC2A 3LY, UK
[12]Department of Oncology, Vascular Patterning Laboratory, KU Leuven, B-3000 Leuven, Belgium
[13]Vesalius Research Center, Vascular Patterning Laboratory, VIB, B-3000 Leuven, Belgium
[14]Vascular Biology Program, IFOM, FIRC Institute of Molecular Oncology Foundation, 20139 Milan, Italy
[15]Co-first author
*Correspondence: patrizia.agostinis@med.kuleuven.be
http://dx.doi.org/10.1016/j.ccr.2014.06.025

SUMMARY

Chloroquine (CQ) has been evaluated as an autophagy blocker for cancer treatment, but it is unknown if it acts solely by inhibiting cancer cell autophagy. We report that CQ reduced tumor growth but improved the tumor milieu. By normalizing tumor vessel structure and function and increasing perfusion, CQ reduced hypoxia, cancer cell invasion, and metastasis, while improving chemotherapy delivery and response. Inhibiting autophagy in cancer cells or endothelial cells (ECs) failed to induce such effects. CQ's vessel normalization activity relied mainly on alterations of endosomal Notch1 trafficking and signaling in ECs and was abrogated by Notch1 deletion in ECs in vivo. Thus, autophagy-independent vessel normalization by CQ restrains tumor invasion and metastasis while improving chemotherapy, supporting the use of CQ for anticancer treatment.

INTRODUCTION

Several clinical trials are evaluating the benefit of the lysosomotropic antimalarial agent chloroquine (CQ), or its derivative hydroxychloroquine, for numerous late-stage cancers, with promising results (http://www.cancer.gov/clinicaltrials) (Maes et al., 2013).

CQ's anticancer activity is believed to rely on blocking cancer cell autophagy, a process whereby molecules and organelles are encapsulated in autophagosomes and delivered to lysosomes, where the cargo is degraded and its building blocks are recycled to preserve homeostasis, especially in metabolic stress (Mizushima et al., 2008). Autophagy in tumors is stimulated in

Significance

The antimalaria drug chloroquine (CQ) is tested in oncology. Its anticancer activity is believed to rely only on the blockade of autophagy in cancer cells, but effects on stromal cells are poorly characterized. We report that besides reducing in vivo cancer cell proliferation by blocking autophagy, CQ targets endothelial cells via autophagy-independent alterations of endosomal Notch1 trafficking, thereby inducing tumor vessel normalization. By tightening tumor vessels and reducing tumor hypoxia, CQ impaired cancer cell invasion and metastasis and enhanced the delivery and response to chemotherapeutics. These findings provide insight into the anticancer mechanisms of CQ and identify CQ as a tumor vessel normalization agent.

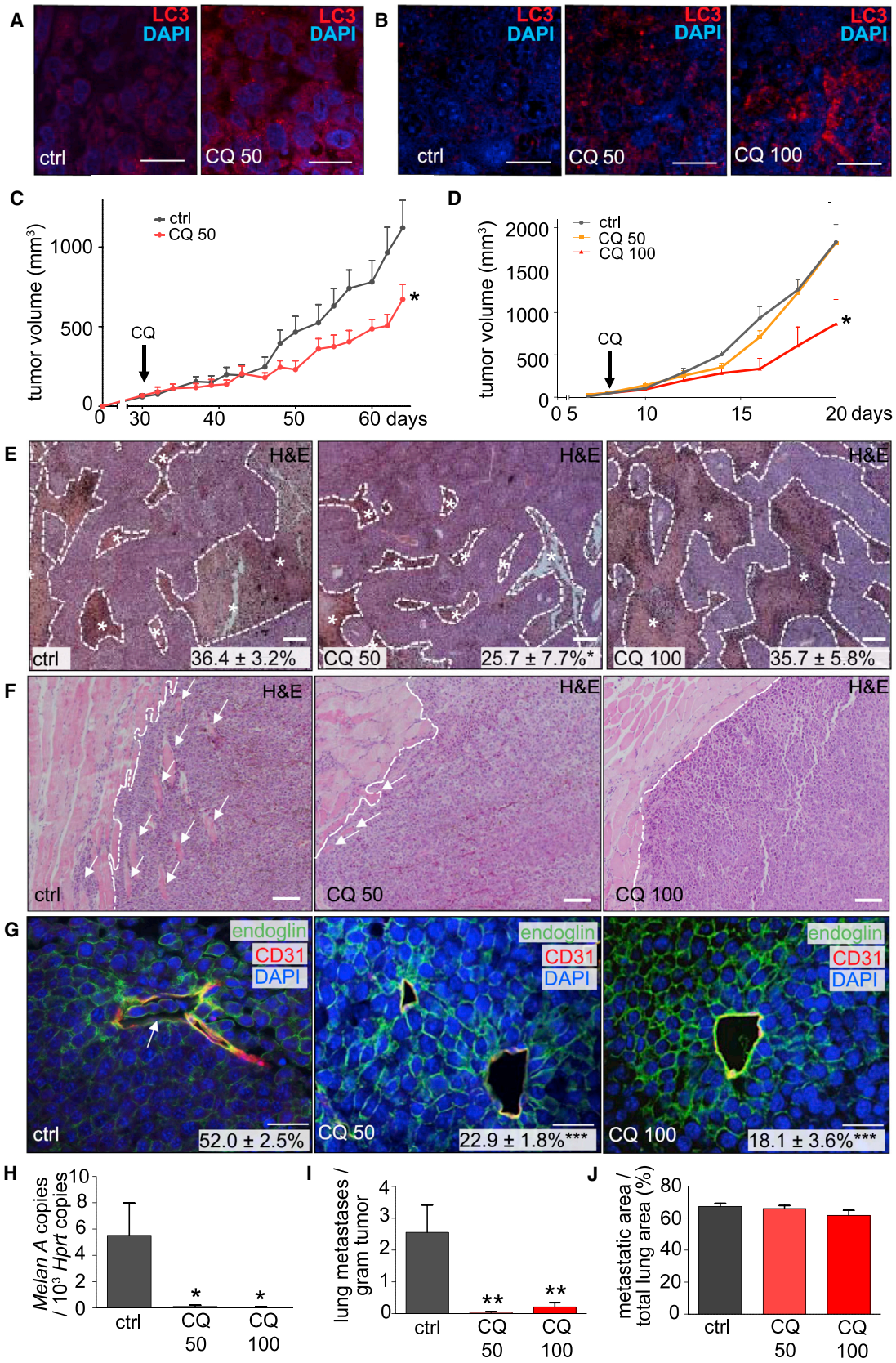

(legend on next page)

nutrient-deprived areas and as a stress response to anticancer treatment. However, the role of autophagy in cancer is context and tumor stage dependent, and the mechanisms underlying the ability of autophagy to modulate invasion and metastasis are ill defined (Maes et al., 2013; White, 2012).

Being a weak base, CQ is trapped upon protonation in acidic compartments, like late endosomes (LEs) and lysosomes, where, by alkalinizing these compartments, it affects fusion events and disrupts endosomal and autophagic cargo degradation. Thus, by blocking lysosomal function, CQ can also act via autophagy-independent mechanisms (Maes et al., 2013), but their nature remains elusive. A better understanding of how CQ enhances therapeutic outcomes of conventional chemotherapeutics is desirable. Here, we investigated whether the anticancer activity of CQ is mediated by autophagy-dependent or autophagy-independent effects on the tumor cells and/or tumor stroma.

RESULTS

CQ Reduces Tumor Growth and Cancer Cell Proliferation

We focused on melanoma because it is poorly treatable and reliant on autophagy for its growth (Xie et al., 2013). Consistent with its autophagy-inhibitory activity, CQ treatment of cancer cells blocked lysosomal degradation of autophagy-selective substrates, as shown by the increased levels of LC3II and p62 (Figures S1A and S1B available online) and elevated numbers and size of $LC3^+$ puncta (Figure S1C). CQ also impaired clonogenic cancer cell expansion and proliferation, while increasing cell death, especially under metabolic stress (Figures S1D–S1I). A375m cells were more sensitive than B16-F10 cells to the cytotoxic activity of CQ (Figures S1F and S1I). Thus, melanoma cells rely on autophagy to sustain growth, and blockage of their heightened autophagic flux by CQ compromises viability.

To evaluate the effects of CQ on tumor progression, we implanted B16-F10 cells and A375m cells in mice. Treatment with 0, 50, or 100 mg/kg/day CQ was initiated when tumors were 100 mm^3; tumors were collected when reaching 1,000 mm^3 (A375m after 9 weeks for control and 12 weeks for CQ) or 2,000 mm^3 (B16-F10 after 20 days for 0 and 50 mg/kg/day CQ or 26 days for 100 mg/kg/day CQ), and further analysis was performed in size-matched tumors. We refer to 50 mg/kg/day as the low dose and to 100 mg/kg/day as the high dose of CQ.

Using an antibody reacting with CQ revealed an immunoreactive signal in tumors, which increased with higher doses of CQ, while no signal was detected in untreated tumors (Figure S1J). Intratumoral CQ levels in vivo detected by gas chromatography-mass spectrometry were largely comparable with those in cancer cells in vitro (Figure S1K). At both doses, CQ reduced the autophagic flux in both tumors, as evidenced by the increased LC3II levels and numbers of $LC3^+$ cells (Figures 1A and 1B; Figures S1L and S1M). In line with the higher sensitivity of A375m cells to CQ, a low dose of CQ reduced A375m tumor growth and cancer cell proliferation in vivo, while only a high dose of CQ reduced these parameters in B16-F10 tumors (Figures 1C and 1D; Figures S1N and S1O).

CQ Reduces Tumor Necrosis In Vivo but Impairs Cancer Cell Invasion, Intravasation, and Metastasis

Surprisingly, however, the low dose of CQ reduced rather than increased cancer cell death in both tumors in vivo, while cancer cell death in B16-F10 tumors was not affected by the high CQ dose (Figure 1E; Figures S1P and S1R). These unexpected findings were likely not due to underdosing of CQ (see above; Figure S1K). Moreover, cancer cells isolated from tumors of CQ-treated mice were still sensitive to CQ treatment in vitro, showing that they had not acquired resistance to CQ (Figures S1S and S1T). The reduced cancer cell death was also not due to a change in the expression of protumorigenic signals (Figure S1U). Thus, contrary to the cytotoxic effect of CQ in vitro, CQ was less toxic for cancer cells in A375m and B16-F10 tumors at a low dose in vivo. The discrepancy between CQ's effects in vitro and in vivo raised the question whether CQ induced cancer cell nonautonomous effects in vivo.

We also explored if CQ affected metastasis. Because pilot experiments showed that B16-F10 (but not A375m) tumors were invasive and metastatic, we used B16-F10 cancer cells. CQ-treated tumors were less invasive and had more sharply demarcated borders at a low dose and even more at a high dose of CQ (Figure 1F). Double staining for the endothelial cell (EC) marker CD31 and for endoglin, labeling melanoma cells and ECs, showed that CQ reduced the fraction of vessels containing cancer cells in their lumen as well as the number of cancer cells inside vessels, suggesting that CQ impaired cancer cell intravasation (Figure 1G). CQ also lowered the number of circulating cancer cells (Figure 1H). Counting of pulmonary metastatic nodules, measuring metastatic nodule size, and calculating the metastatic index revealed that CQ dose-dependently impaired metastasis (Figure 1I; Figure S1V). However, CQ did not alter cancer cell invasion in Matrigel in vitro (Figure S1W) and did not alter colonization of B16-F10 cells to the lungs after intravenous injection in an experimental metastasis model (Figure 1J). Thus, the

Figure 1. Effect of CQ on Tumor Necrosis, Intravasation, and Metastasis

(A and B) Immunostaining for LC3 in A375m (A) or B16-F10 (B) tumors from control (ctrl)-treated mice or from mice treated with a dose of 50 or 100 mg/kg/day CQ.

(C and D) Growth curve of A375m xenografts (n = 11; C) or B16-F10 tumors (n = 20; D) in ctrl- and CQ-treated mice.

(E) Necrotic areas (asterisks within dashed lines) in B16-F10 tumors after CQ versus ctrl (hematoxylin and eosin [H&E] staining); quantification of the necrotic area is indicated (percentage of total; n = 8–11).

(F) H&E staining of ctrl- and CQ-treated B16-F10 tumors. Arrows indicate residual muscle tissue. Dashed line indicates tumor border.

(G) Immunostaining for CD31 and endoglin of ctrl- and CQ-treated B16-F10 tumors. Quantification of the percentage of vessels with intraluminal tumor cells ($CD31^-endoglin^+$; arrows) is indicated (n = 8).

(H) RT-PCR analysis for *Melan A* in blood samples as a measure of circulating tumor cells in B16-F10 tumor-bearing mice treated with CQ or PBS (n = 10–15).

(I) Metastatic index in B16-F10 tumor-bearing mice treated with CQ or PBS (n = 14–18).

(J) Quantification of metastatic nodule area expressed as a percentage of total lung area from ctrl- and CQ-treated mice 14 days after tail vein injection of 200,000 cells (n = 14–18).

Scale bars represent 50 μm (A and B), 100 μm (E and F), and 25 μm (G). All quantitative data are mean ± SEM. *$p < 0.05$; **$p < 0.01$. See also Figure S1.

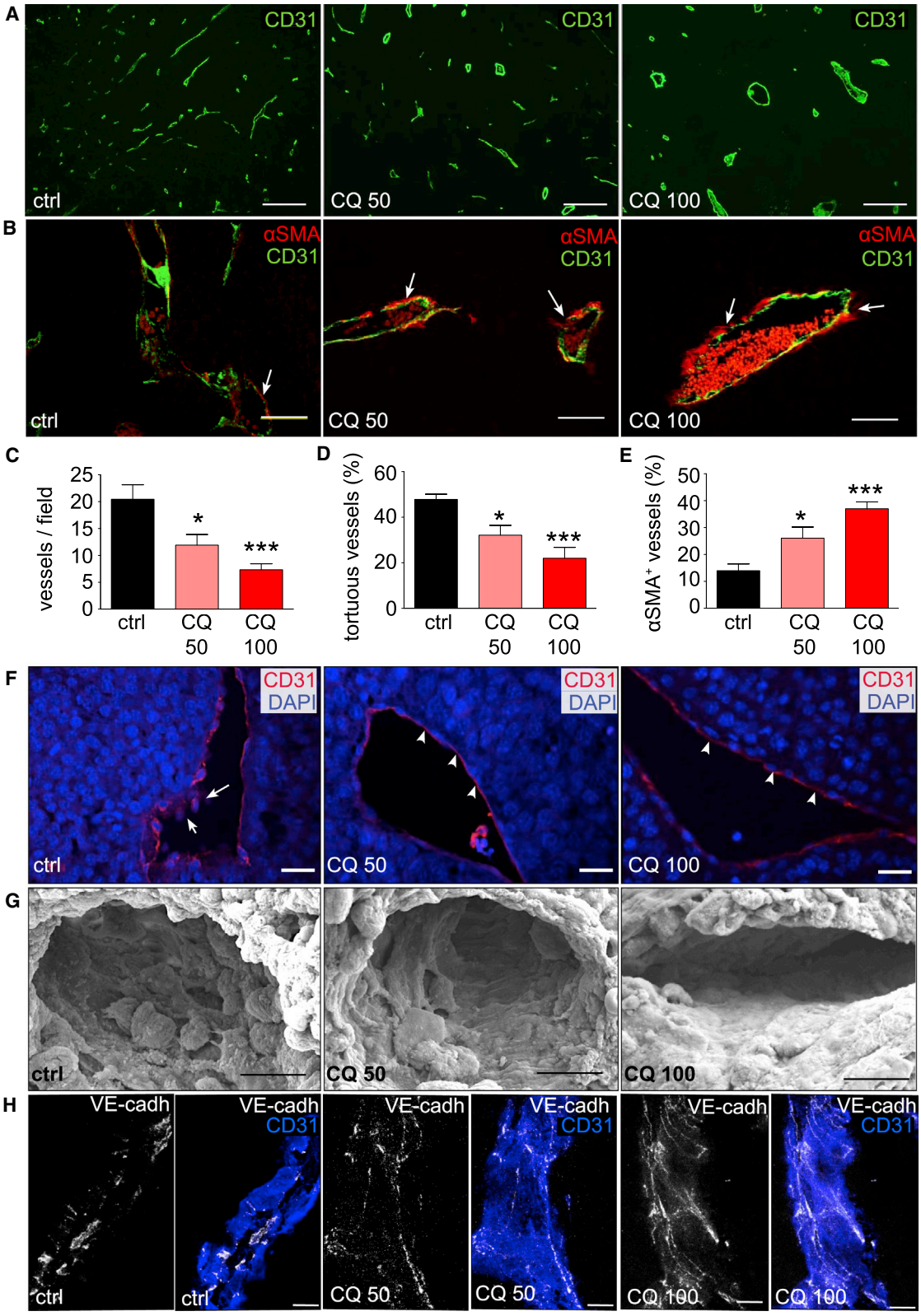

Figure 2. Effect of CQ on Vessel Structure and Maturation In Vivo

(A–E) B16-F10 tumors from CQ-treated and ctrl mice were immunostained for CD31 (A and B) and αSMA (B) and quantified for tumor vessel density (C) (n = 5), percentage of tortuous vessels (D) (n = 5), and pericyte-covered vessels (E) (n = 5 or 6).

(legend continued on next page)

antimetastatic effects of CQ are likely not mediated by a direct effect on the cancer cells themselves. We then explored if effects on stromal cells could explain the reduced invasion and metastasis by CQ. However, CQ did not affect the infiltration of $CD45^+$ leukocytes (Figure S1X) and did not alter the accumulation of platelet-derived growth factor receptor α ($PDGFR\alpha^+$)-positive or α-smooth muscle actin (αSMA^+)-positive cancer-associated fibroblasts (not shown). Because CQ reduced tumor cell intravasation and tumor vessels can affect metastasis, we explored if CQ altered structural and functional properties of tumor vessels.

CQ Induces Tumor Vessel Normalization and Improves Tumor Vessel Function

A hallmark of many cancers is a structurally and functionally abnormal vasculature, which reduces tumor perfusion and enhances hypoxia, invasion, and metastasis (Carmeliet and Jain, 2011). Indeed, CD31 staining revealed that the vascular architecture in human melanoma biopsies was more chaotic, complex, and disordered than in healthy skin (Figure S2A). Double staining for CD31 and the mural cell markers αSMA showed that fewer pericytes covered blood vessels in human melanoma than in healthy skin, indicating more immature tumor vessels (Figure S2A), another sign of vessel disorganization.

Because CQ increased cancer cell death in stressed conditions in vitro, we explored if the antimetastatic effect of CQ in vivo was due to an increased supply of oxygen and nutrients and improved EC barrier function via vessel normalization (Carmeliet and Jain, 2011). Indeed, CQ dose-dependently decreased tumor vessel density and tortuosity in B16-F10 tumors (Figures 2A, 2C, and 2D). Whole-mount CD31 staining of thick tumor sections showed that the vascular architecture was less chaotic and complex in CQ-treated tumors (Figure S2B). CQ also dose-dependently improved vessel coverage by pericytes, a sign of vessel maturation (Figures 2B and 2E). The vessel normalization effects of CQ were even more pronounced at a high dose of CQ (Figures 2A–2E).

We also analyzed the EC morphology in tumor vessels by CD31 staining. Control tumors had thick, irregular vessel walls with EC extensions protruding in the lumen, whereas CQ-treated vessels had thin walls with more uniform alignment of ECs (Figure 2F). Scanning electron microscopy showed a regular, flat monolayer of ECs in CQ-treated tumor vessels, in contrast to the more irregular and chaotically organized EC lining in control vessels (Figure 2G). CQ also increased vascular endothelial (VE)-$cadherin^+$ adherens junctions in tumor vessels (Figure 2H). The EC alignment and increase in adherens junctions after CQ treatment make the EC barrier more impenetrable, which could explain the reduced cancer cell intravasation upon CQ treatment. A comparable vessel normalization phenotype was observed in human A375m melanoma xenografts (Figures S2C–S2H), indicating that the vascular effects of CQ were not influenced by the (human or murine) type of malignant cell or the absence of T cell-mediated immunity.

To analyze vessel functionality, we injected tumor-bearing mice with lectin-fluorescein isothiocyanate (FITC) to label perfused vessels or dextran-FITC to measure leaky vessels and then stained B16-F10 and A375m tumor sections for CD31 to identify all vessels (perfused and nonperfused) so that the percentage of perfused and leaky vessels could be determined. CQ increased the fraction of perfused lectin-$FITC^+$ $CD31^+$ vessels (Figure 3A; Figures S3A and S3B), while reducing dextran-FITC leakage (Figure 3B). CQ also dose-dependently decreased tumor hypoxia (Figure 3C; Figures S3C and S3D). Overall, CQ improved tumor vessel functionality. The metabolically less stressed tumor milieu, which renders cancer cells less dependent on autophagy, likely explains why tumor necrosis was reduced when mice were treated with a low dose of CQ (Figure 1E; Figure S1P). At a high CQ dose, the prosurvival effect of vessel normalization was balanced by the increased cytotoxic effect of CQ, explaining why cancer cell death was no longer reduced, but comparable with control (see above).

CQ Increases the Delivery and Efficacy of Chemotherapy

Tumor vessel normalization improves the delivery and efficacy of chemotherapeutics (Carmeliet and Jain, 2011). Therefore, we explored if pretreatment with low-dose CQ improved the delivery and cytotoxicity of cisplatin (CPt). CQ treatment was initiated when tumors reached 50 mm^3 and was repeated daily for 6 days to induce vessel normalization before the administration of a single dose of CPt (10 mg/kg) and assessment of CPt-DNA adduct formation. CQ increased CPt-DNA adducts in tumors (Figures 3D and 3E), suggesting improved delivery of the cytotoxic drug, in line with the increased tumor perfusion.

We then explored whether CQ enhanced the anticancer effect of a suboptimal CPt dose (2.5 mg/kg every other day). Compared with CPt monotherapy, the combination of CQ with this dose of CPt caused an anticancer effect accompanied by increased necrosis (Figures 3F and 3G; Figure S3E). The metastatic index decreased most when CQ was combined with CPt, but the small number of metastatic nodules upon CQ monotherapy precluded us from obtaining a higher significance level (Figure 3H). However, CQ did not increase the in vitro cytotoxic efficacy of CPt (Figure 3I), suggesting that chemosensitization by CQ in vivo was due to effects on vessel normalization (drug delivery). Similar results in vivo were obtained when combining dacarbazine (40 mg/kg) with CQ (Figures S3F and S3G).

ATG5 Silencing in Cancer Cells Does Not Phenocopy CQ's Effects

To assess if the tumor and vessel phenotypes of CQ were attributable to blockade of autophagy in cancer cells, we reduced the protein levels of the essential autophagy factor ATG5 in B16-F10 cells (by 87 ± 3%; $n = 3$; $p < 0.005$). ATG5 silencing reduced baseline autophagy in cancer cells in vitro and in vivo (Figure 4A; Figure S4A). Similar to CQ, ATG5 silencing reduced cancer cell

(F) Confocal images of CD31 immunostaining of the vascular network of ctrl- and CQ-treated B16-F10 tumors. Arrows indicate ECs protruding into the vessel lumen; arrowheads indicate smooth thin endothelial lining.
(G) Scanning electron microscopy of B16-F10 tumor vessels from ctrl- and CQ-treated mice.
(H) Double staining for VE-cadherin (VE-cadh) and CD31 of B16-F10 tumors from ctrl- and CQ-treated mice.
Scale bars represent 100 μm (A), 50 μm (B, F, and H), and 5 μm (G). All graphs show mean ± SEM. *$p < 0.05$; ***$p < 0.001$. See also Figure S2.

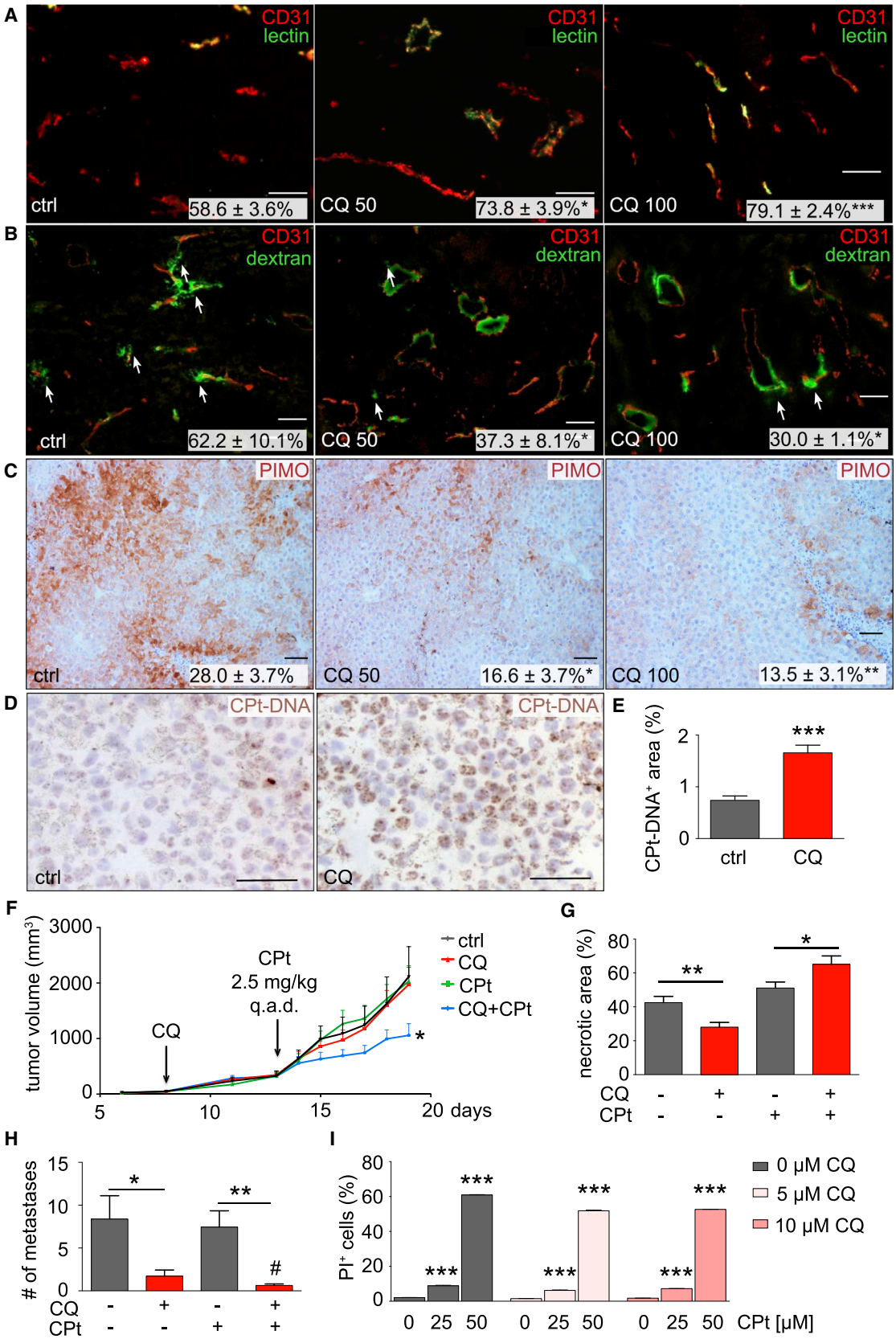

(legend on next page)

proliferation and colony formation and increased cell death in vitro, especially in metabolic stress (Figures S4B–S4D).

Inhibition of cancer cell-intrinsic autophagy by ATG5 silencing reduced tumor growth and metastasis (Figure 4B; Figure S4E). However, ATG5-silenced tumors had larger regions of necrosis, and only the first 10 layers of perivascular cancer cells survived, likely because cancer cells located more distantly from vessels were unable to cope with the increased metabolic stress (Figures 4C and 4D). Intriguingly, ATG5-silenced tumors displayed prominent signs of invasion (Figure 4E) and intravasation (Figures 4F and 4G), comparable with control tumors. Also, ATG5-silenced cancer cells were nearly unable to colonize the lungs after intravenous injection (Figure 4H), suggesting that their ability to survive and colonize was reduced when cancer cell-intrinsic autophagy was compromised, confirming a recent report (Peng et al., 2013) and explaining the reduced metastatic potential of ATG5-silenced B16-F10 tumors.

Importantly, however, ATG5 silencing did not promote tumor vessel normalization (Figures 4I–4K) and did not improve tumor perfusion and oxygenation (Figures 4L and 4M; Figures S4F and S4G). In fact, vessel tortuosity was increased in ATG5-silenced tumors (Figure 4I; Figure S4G). Thus, like CQ-treated tumors, autophagy-incompetent cancer cells grew and metastasized less, but silencing of ATG5 in cancer cells induced effects on tumor vessels in vivo that were opposite to those induced by CQ.

CQ-Mediated Vessel Normalization Is Independent of EC Autophagy

Tumor vessel normalization can result from an indirect effect on the angiogenic activity of cancer cells or from a direct effect on ECs. Because CQ did not alter the production of angiogenic molecules by cancer cells in vivo (Figure S5A), we studied if CQ affected ECs in vitro. CQ increased LC3II and p62 levels in ECs, indicating that it blocked autophagic flux (Figure S5B), although this increase was less pronounced than in cancer cells.

We monitored CQ's effects on EC processes using the EC spheroid sprouting model. In control conditions, CQ decreased the number and length of the sprouts (Figures 5A–5C). Spheroids formed more sprouts in hypoxia and fewer sprouts upon starvation, but CQ reduced vascular sprouting in both conditions (Figures S5C–S5H). Also, CQ decreased EC migration and proliferation (Figures S5I and S5J) and induced EC death only at high concentrations in metabolic stress (ischemia; Figure S5K). The effects of CQ on ECs can explain its ability to reduce tumor vessel density and to induce vessel normalization.

We next explored if CQ's vessel normalization effect was due to autophagy inhibition in ECs. We first assessed if ATG5 silencing in ECs reproduced the vascular phenotype induced by CQ. Lentiviral transfer of an ATG5-specific small hairpin RNA (shRNA) lowered ATG5 protein levels by 69% to 75% ($n = 6$; $p < 0.05$) and decreased LC3II formation (Figure S5L). However, ATG5 silencing did not reduce vessel sprouting (Figures S5M–S5O) and did not affect EC proliferation and migration, or cell death, except moderately in metabolic stress (Figures S5P and S5R).

To explore the role of EC autophagy in vivo, we used $Atg5^{EC\text{-}KO}$ mice lacking *Atg5* in ECs, obtained by intercrossing $Atg5^{lox/lox}$ mice (Hara et al., 2006) with *VE-cadherin-Cre* mice (Oberlin et al., 2010) and appearing healthy in baseline conditions. B16-F10 tumor growth was reduced in $Atg5^{EC\text{-}KO}$ mice, but the metastatic index was similar (Figures 5D and 5E). *Atg5* deletion in ECs did also not affect tumor necrosis and hypoxia (Figures 5F and 5G) and, importantly, did not induce tumor vessel normalization (Figures 5H–5O; Figure S5S). In fact, tumor vessels in $Atg5^{EC\text{-}KO}$ mice were smaller, more numerous and tortuous (Figures 5H, 5J, and 5K), had an abnormal EC lining (Figure S5S), and were less mature and perfused (Figures 5I and 5M–5O). Thus, EC-specific deletion of *Atg5* caused a tumor vessel phenotype that is opposite to that induced by CQ.

CQ Promotes Accumulation of Notch1 in LEs of ECs

Because the in vivo effects of CQ on tumor vessel normalization could not be ascribed to the inhibition of autophagy in ECs, we investigated how CQ altered EC biology. By virtue of its alkalinizing effect on lysosomes, CQ not only inhibits the degradation of autophagosomes by lysosomes but also interferes with the endosomal degradative route. We therefore stained ECs for early endosome (EE) antigen 1 (EEA-1) (a marker of EEs), Rab-11 (labeling recycling endosomes [REs]), and CD63 and LAMP1 (markers of LEs, multivesicular bodies (MVBs), and lysosomes). CQ did not affect the EE or RE pool, indicating that recycling routes from EEs to the surface were not affected, but caused a substantial expansion and swelling of the more acidic LEs, MVBs, and lysosomes (Figures 6A–6F; Figures S6A and S6B).

Because endosomes are emerging as platforms regulating signaling through receptor internalization (Baron, 2012), we screened a panel of angiogenic molecules related to vessel normalization, focusing on transmembrane proteins known to cycle via endosomal compartments (Eichmann and Simons, 2012). Using CD63 to mark LEs, we explored which molecules colocalized in LEs after CQ treatment by determining the Pearson correlation (PC) coefficient (a biologically significant colocalization requires a PC coefficient > 0.5). CQ increased LE colocalization of VE growth factor receptor 1, VE growth factor

Figure 3. Effect of CQ on Vessel Function and Tumor Chemosensitivity

(A) Micrographs of lectin-FITC-perfused and CD31-stained vessels in ctrl- and CQ-treated B16-F10 tumors. Quantification of perfusion is indicated ($CD31^+$lectin$^+$ area, percentage of total $CD31^+$ area) ($n = 5–7$).

(B) Micrographs of FITC-dextran-perfused and CD31-immunostained vessels in ctrl- and CQ-treated B16-F10 tumors. Arrows indicate sites of vascular leakage. Quantification of leakage is indicated ($CD31^-$dextran$^+$ area, percentage of total dextran$^+$ area) ($n = 4$ or 5).

(C) Micrographs of pimonidazole (PIMO) staining (brown) of hypoxic zones in ctrl- and CQ-treated B16-F10 tumors. Quantification of $PIMO^+$ area as a percentage of tumor area is indicated ($n = 7–12$).

(D and E) Immunostaining for CPt-DNA adducts in ctrl- and CQ-pretreated (50 mg/kg/day) B16-F10 tumors (D) and quantification (E) ($n = 9$).

(F–H) B16-F10 tumor growth rate (F), tumor necrosis (G), and pulmonary metastasis (H) upon single or combined treatment with CQ and CPt (2.5 mg/kg) ($n = 12–15$). $^{\#}p = 0.07$ relative to CQ alone.

(I) Quantification of the fraction of PI^+ dead B16-F10 cancer cells in vitro upon CPt treatment in the presence of increasing concentrations of CQ ($n = 3$).

Scale bars represent 100 μm (A–C) and 50 μm (D). All quantitative data are mean ± SEM. *$p < 0.05$; **$p < 0.01$; ***$p < 0.001$. See also Figure S3.

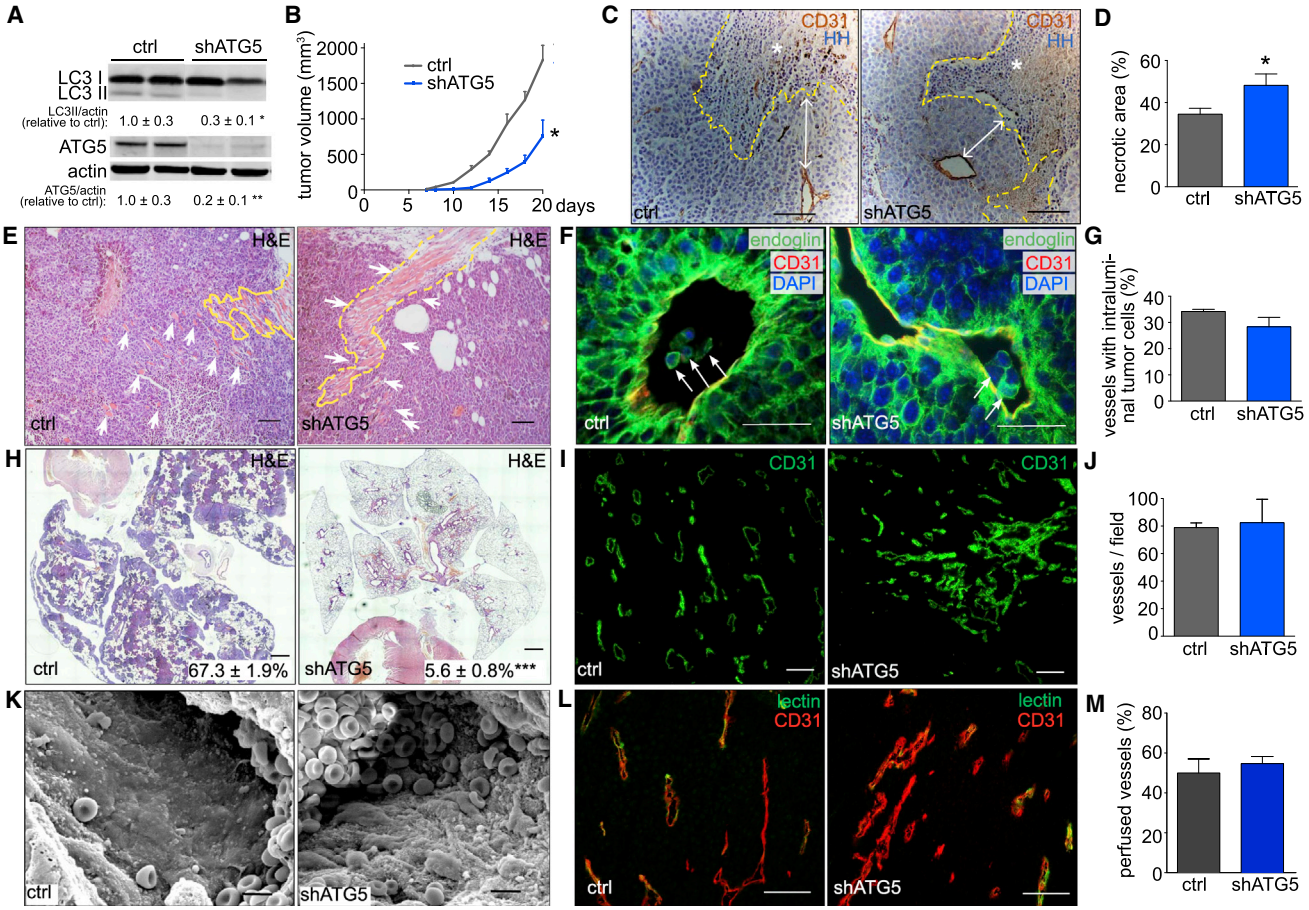

Figure 4. Effect of ATG5 Silencing in Tumor Cells on Tumor Growth, Invasion, and Metastasis

(A) Immunoblotting for LC3 and ATG5 protein levels relative to actin in lysates from B16-F10 cancer cells transduced with a shRNA-ATG5 expressing lentivirus (shATG5) or empty vector (ctrl). Densitometric quantifications of LC3II levels and ATG5 protein levels, relative to actin, are shown (n = 6–8 and n = 7 or 8, respectively).

(B) Growth curve of primary B16-F10 tumors generated with ctrl or shATG5 cells (n = 9–15).

(C and D) Immunostaining for CD31 and Harris hematoxylin (HH) nuclear counterstaining in ctrl and shATG5 B16-F10 tumors (C) and quantification of the necrotic area (D). White arrows indicate distance of vessels (CD31 staining) from the necrotic area (asterisk). The border between the viable and necrotic tumor area is demarcated with a dashed yellow line (n = 9–11).

(E) H&E staining on B16-F10 tumor cells (arrows indicate residual muscle tissue) in ctrl versus shATG5 tumors. The dotted yellow lines demarcate the border between the tumor and surrounding muscle.

(F and G) Double immunostaining for CD31 and endoglin of ctrl and shATG5 B16-F10 tumors (F) and quantification of the percentage of vessels with intraluminal tumor cells ($CD31^{-}endoglin^{+}$; arrows) (G) (n = 3; p = NS).

(H) Representative micrographs of lung metastasis after tail vein injection of ctrl or shATG5 B16-F10 tumor cells (H&E staining). Quantification of metastatic area (percentage of total lung area) is indicated (n = 5).

(I and J) Immunostaining for CD31 of ctrl and shATG5 B16-F10 tumors (I) and quantification (J) (n = 5 or 6).

(K) Scanning electron microscopy of the endothelial lining of vessels from ctrl and shATG5 B16-F10 tumors.

(L and M) Double immunostaining for CD31 and lectin of ctrl and shATG5 B16-F10 tumors (L) and quantification of percentage $CD31^{+}lectin^{+}$ vessel area (M) (n = 5–7).

Scale bars represent 200 μm (C and I), 100 μm (E), 50 μm (L), 25 μm (F), 5 μm (K), and 1 mm (H). All quantitative data are mean ± SEM. *p < 0.05. See also Figure S4.

receptor 2, and PDGFRα, while decreasing colocalization of VE-cadherin, but their PC coefficients were <0.4 (Figure 6G). CQ reduced VE-cadherin colocalization in LEs but increased its cell surface levels (Figure 6G; Figures S6C and S6D), consistent with the in vivo findings in CQ-treated tumor vessels (Figure 2H).

Of all tested molecules, Notch1 was the one that after CQ co-localized primarily in LEs (but not in EEs) and had the highest PC coefficient (0.66 ± 0.01), as evidenced by immunostaining using an antibody against the carboxyl terminus of Notch1 (Figures 6G and 6H; S6E-H). This finding was interesting because the vessel normalization phenotype induced by CQ is similar to the phenotype observed by Notch1 activation in tumor ECs (Li et al., 2007). Indeed, Notch1 promotes EC quiescence (Zhang et al., 2011), and its inhibition evokes vascular remodeling and hyperbranching (Dill et al., 2012; Liu et al., 2011; Yan et al., 2010), properties that could explain CQ's vessel normalization effects if its activity relied on Notch1 activation. We therefore focused on the role of Notch1 signaling in the CQ-mediated vascular effects.

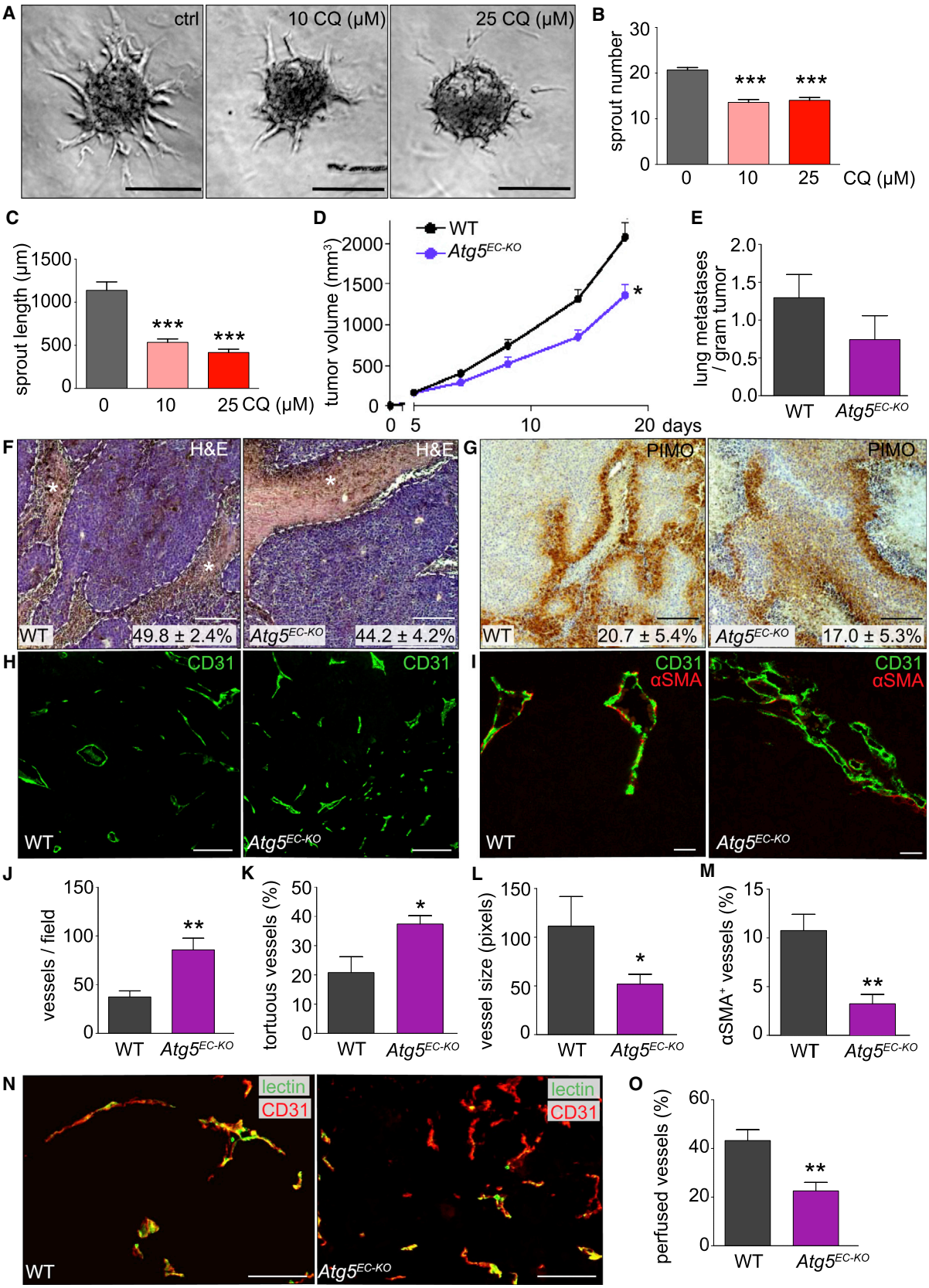

(legend on next page)

CQ Alters Endosomal Trafficking of Notch1

Notch1 undergoes proteolysis by ADAM sheddases and γ-secretase at the cell surface as well as in EEs and LEs and MVBs upon internalization and endosomal routing (De Strooper and Annaert, 2010; Sannerud and Annaert, 2009). Briefly, ligand binding to the cell surface-exposed Notch1 extracellular domain, which forms a heterodimer with the p120 transmembrane Notch1 fragment, facilitates ectodomain shedding of p120. The newly generated Notch1 extracellular truncation (NEXT) fragment is further processed by γ-secretase, likely during endosomal routing, releasing the Notch1 intracellular domain (NICD) that translocates to the nucleus to regulate transcription (Fortini, 2009).

Because CQ did not alter *NOTCH1* transcript levels (Figure S6I), we focused on other mechanisms to explain Notch1 accumulation in LEs and MVBs after CQ administration. Immunoblotting showed that CQ dose-dependently increased the levels of the NEXT fragment, accompanied by a concomitant increase in NICD, while the full-length 300 kDa (p300) and the p120 kDa Notch1 species were barely affected (Figure 6I). Cell surface biotinylation assays revealed that the plasma membrane levels of p120 were only slightly affected, while NEXT was undetectable at the surface (Figure 6J), suggesting that initial endosomal routing between the cell surface and EEs was not altered by CQ and that p120 processing to NEXT occurred downstream of the constitutive ADAMs-mediated shedding, after internalization "en route" to or within endosomal compartments.

In line, blockage of endocytosis by Dynasore reduced the CQ-induced Notch1 accumulation in LEs (Figures 6K and 6L). As the V-ATPase inhibitor bafilomycin A1 (Baf), which like CQ also neutralizes the acidic pH in LEs and lysosomes, increased the colocalization of Notch1 in LEs (Figures 6M and 6N), these results support a model whereby, following Notch1 internalization and endosomal trafficking, CQ caused NEXT accumulation in LEs.

CQ Increases Notch1 Signaling in ECs

We then analyzed if the CQ-induced accumulation of Notch1 in LEs/lysosomes caused any changes in NICD signaling. CQ time-dependently increased NICD protein levels (Figure 7A; Figure S7A). The magnitude of this increase was lower than the induction by a high concentration (2 μg/ml) of the Notch1 ligand DLL4 in ECs, but comparable with that induced by a more physiological concentration of DLL4 (0.5 μg/ml) (Guarani et al., 2011; Harrington et al., 2008) (Figure 7A; Figure S7A). DLL4 induced an acute but more transient increase in NICD levels, associated with rapid processing of p120, while CQ caused a slower but more sustained elevation of NICD over 72 hr (Figure 7A; Figures S7A and S7B). NICD formation after CQ was blunted by the γ-secretase inhibitors DAPT (Figure S7C) and Inhibitor X, a finding confirmed in cells lacking presenilin-1 and presenilin-2, the catalytic components of γ-secretase (not shown).

These data imply that NICD formation by CQ relies on NEXT processing by γ-secretase but do not explain why NEXT accumulated after CQ (Figure 7A; Figure S7D). Because CQ did not affect γ-secretase directly, measured with an in vitro enzymatic activity assay (Figure S7E), we hypothesized that by impairing lysosomal degradation, CQ caused NEXT to accumulate in LEs and lysosomes while concurrently providing a pool of substrate for γ-secretase to generate NICD. We thus analyzed the half-life of endogenous NEXT and NICD in control, DLL4, and CQ conditions in the presence of the protein synthesis inhibitor cycloheximide. Using cycloheximide-treated cells, we also compared control and DAPT treatments to assess the role of decreased lysosomal degradation versus γ-secretase-mediated processing in the turnover of these Notch1 products.

Quantitative immunoblot densitometry showed that the turnover of NEXT and NICD after DLL4 was rapid, consistent with the reported fast and sequential processing of Notch1 by ADAMs and of NEXT by γ-secretase after ligand stimulation (Andersson et al., 2011). In line with the aforementioned data, DAPT reduced the processing of NEXT to NICD in DLL4-stimulated cells (Figures S7F–S7J). In CQ-treated cells, NEXT and NICD levels also declined over time, but with slower kinetics. Importantly, however, DAPT further stabilized the CQ-induced NEXT levels while concomitantly reducing its processing to NICD (Figures S7F–S7J). Thus, because NEXT accumulates in CQ-treated ECs because of reduced lysosomal degradation (prolonging its half-life) and NEXT is the substrate of γ-secretase, the latter is able to generate larger amounts of NICD.

The predominant NICD bands generated in response to DLL4 displayed a slower SDS-PAGE mobility pattern than the one formed after CQ (Figure 7A), suggesting distinct posttranslational modifications (Fortini, 2009), a model we explored by using the proteasome inhibitor lactacystin. In control and DLL4-treated conditions, lactacystin evoked an accumulation of NICD bands with a similar slower mobility pattern (Figure S7K). In contrast, after CQ administration, the faster migrating NICD form that predominantly accumulates over time was not increased by lactacystin (Figure S7K). These results combined with the shorter half-life of NICD in DLL4 conditions (Figures S7F–S7J) suggest that the upper bands represent posttranslational modifications of NICD (possibly phosphorylation, ubiquitinylation) known to target NICD for proteasomal degradation (Andersson et al., 2011). They

Figure 5. Effect of *Atg5*-EC Knockout on Tumor Growth, Invasion, and Metastasis

(A–C) Representative micrographs of EC spheroid sprouting (A) and quantification of sprout number (B) and sprout length (C) in the absence or presence of 10 or 25 μM CQ (n = 19–21).

(D) Growth curve of B16-F10 tumor cells injected into WT or $Atg5^{EC\text{-}KO}$ mice (n = 23–32).

(E) Metastatic index in wild-type (WT) and $Atg5^{EC\text{-}KO}$ mice (n = 21–28).

(F) Necrotic areas (asterisks within dashed line) in B16-F10 tumors in WT and $Atg5^{EC\text{-}KO}$ mice (H&E staining); quantification of the necrotic area is indicated (percentage of total; n = 10).

(G) Representative micrographs of PIMO staining in B16-F10 tumors from WT and $Atg5^{EC\text{-}KO}$ mice. Quantification of $PIMO^{+}$ hypoxic area is indicated (percentage of total; n = 6–9).

(H–M) Immunostaining for CD31 (H) and double immunostaining for CD31 and αSMA (I) of B16-F10 tumors in WT and $Atg5^{EC\text{-}KO}$ mice and quantification of tumor vessel density (J) (n = 4), percentage of tortuous vessels (K) (n = 4), vessel size (L) (n = 4), and percentage of pericyte-covered vessel (M) (n = 6).

(N and O) Double immunostaining for CD31 and lectin of B16-F10 tumors in WT and $Atg5^{EC\text{-}KO}$ mice (N) and quantification of % $CD31^{+}lectin^{+}$ vessel area (O) (n = 5).

Scale bars represent 200 μm (F–H), 10 μm (I), and 100 μm (A and N). All quantitative data are mean ± SEM. *p < 0.05; **p < 0.01; ***p < 0.001. See also Figure S5.

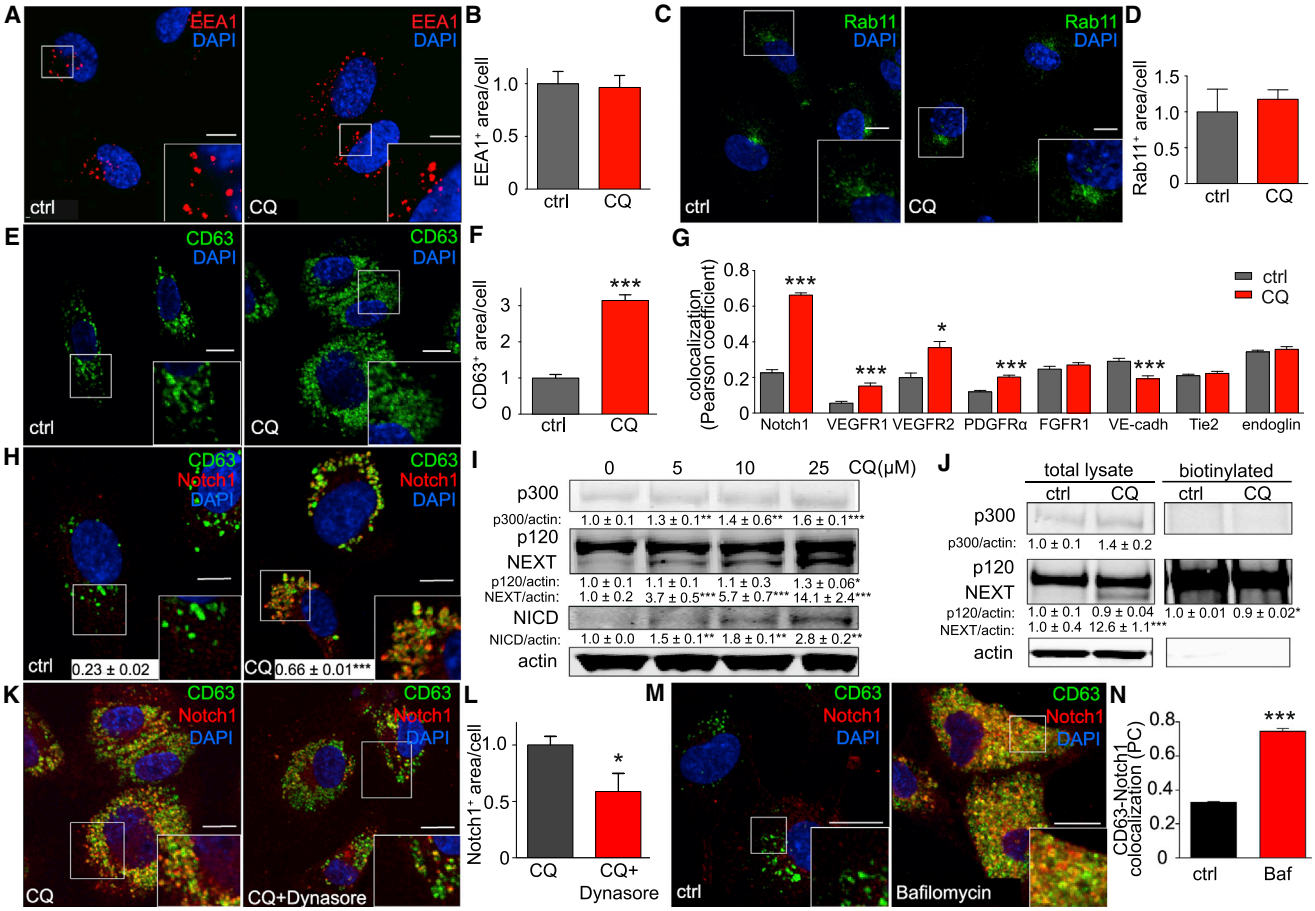

Figure 6. Effect of CQ on Notch1 Localization and Signaling in the LEs

(A–F) Immunostaining (A, C, and E) and quantifications (B, D, and F) of ECs for the early endosomal marker EEA-1 (A and B), the recycling endosomal marker Rab11 (C and D), or the late endosomal compartment (LE/MVB) marker CD63 (E and F). Insets in (A), (C), and (E): Larger magnification of boxed areas (n = 10).

(G) Quantification of the colocalization of CD63 and angiogenic molecules upon double immunostaining (n = 10).

(H) Double immunostaining for Notch1 (using the C-terminal anti-Notch1 antibody) and CD63 in ctrl- and 25 μM CQ-treated HUVECs. Insets: Larger magnification of the boxed areas. The quantification of the colocalization (PC coefficient) is indicated (n = 10).

(I) Immunoblotting of EC lysates for different Notch1 cleavage products in ECs treated with CQ (5–25 μM). Densitometric quantification for the different CQ concentrations relative to control (0) is indicated (n = 3).

(J) Immunoblotting for different Notch1 cleavage products of total EC lysates and biotin-bound fraction of ECs treated with CQ (25 μM) and subjected to cell surface biotinylation before extraction. Densitometric quantification of CQ relative to ctrl is indicated (n = 4).

(K and L) Double immunostaining for Notch1 and CD63 (K) and quantification of Notch1$^+$ area (L) of ECs in ECs treated with 25 μM CQ alone or in combination with the endocytosis blocker Dynasore. Insets: Larger magnification of the boxed areas (n = 10).

(M and N) Double immunostaining (M) and quantification (colocalization) (N) for Notch1 and CD63 of ctrl and the V-ATPase inhibitor Baf-treated ECs. Insets: Larger magnification of the boxed areas (n = 10).

Scale bars represent 10 μm in all micrographs. All quantitative data are mean ± SEM. *p < 0.05; **p < 0.01; ***p < 0.001. See also Figure S6.

also suggest that the NICD form after DLL4 may be more rapidly processed, while the NICD form after CQ may be less prone to proteasomal degradation, an assumption requiring confirmation.

Despite these differences, NICD generated after CQ accumulated in the nucleus and was transcriptionally active, as analyzed by immunoblotting, immunostaining, and use of a NICD luciferase reporter assay (Figures 7B–7D). Moreover, increased mRNA levels of the Notch1-target genes *HEY1* and *HES1* (Figures 7E and 7F) and a pHES-1 luciferase reporter assay (Figure S7L) confirmed that CQ and DLL4 elevated Notch1 signaling with kinetics reflecting those of NICD induction following each particular treatment. Baf also increased nuclear accumulation of NICD (Figure S7M), further strengthening the finding that NICD levels are elevated by compromising lysosomal function. CQ's effect on NICD was specific, as CQ did not affect the levels of the Notch1 ligands DLL4 or Jagged-1 (Figure S7N). In line with reports that Notch signaling in melanoma is constitutively activated by oncogenic signals (Müller, 2012), CQ did not elevate NICD levels in melanoma cells at concentrations that were effective in ECs (not shown).

Notch1 Signaling in ECs Is Required for CQ-Induced Vessel Normalization

To verify the importance of Notch1 in mediating CQ's effects on ECs, we silenced Notch1 and blocked NICD production (and

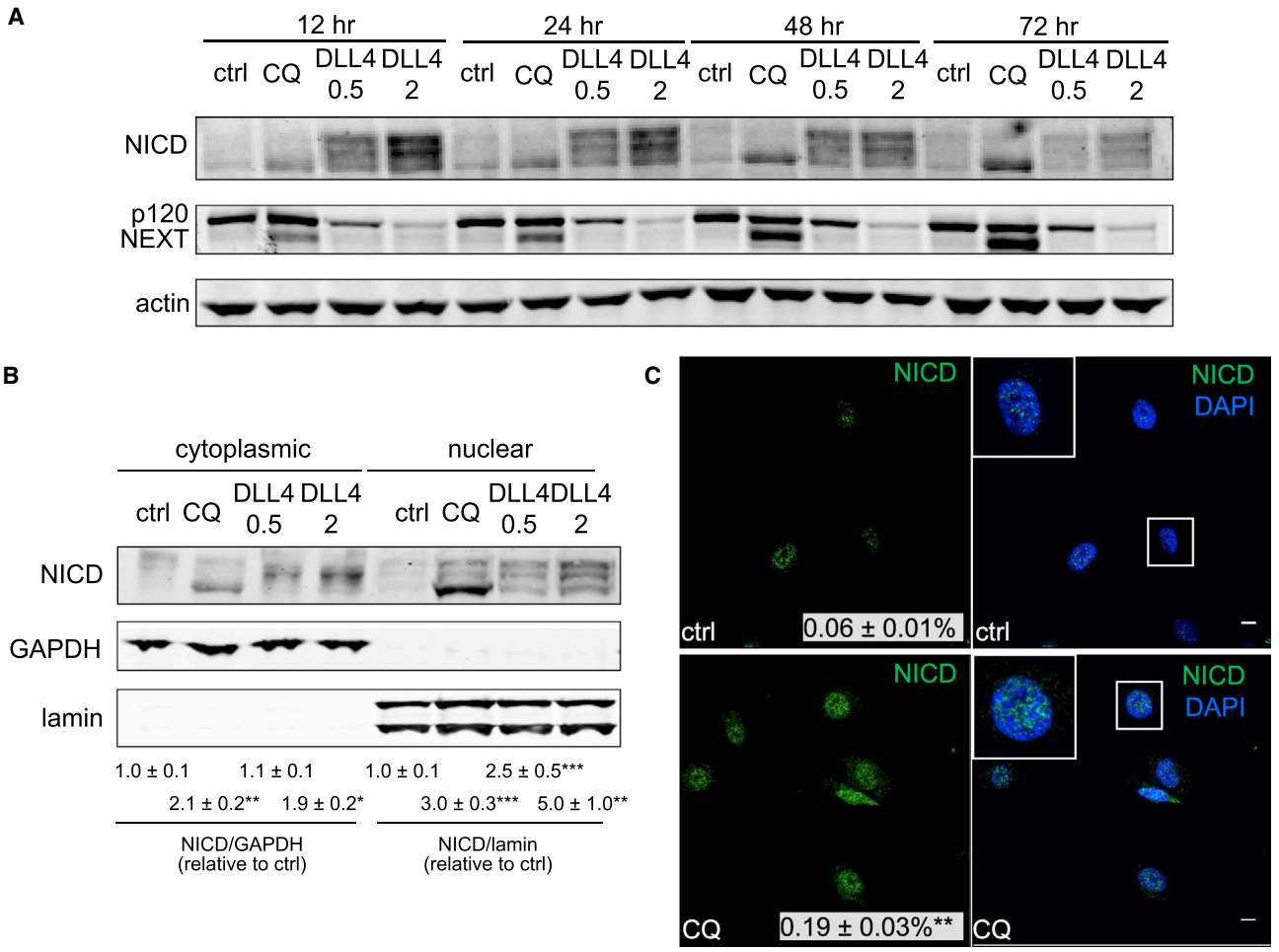

(legend on next page)

thus its signaling) by DAPT. Both Notch1 silencing and DAPT abolished CQ-mediated induction of NICD (Figures S7C and S7O) and CQ's inhibitory effect on vessel sprouting in EC spheroids (Figure 8A; Figures S8A and S8B), thus validating Notch1 as a major target of CQ in ECs. Silencing of the other Notch receptors did not abrogate CQ's inhibitory effects on vessel sprouting (Figures S8C–S8F).

To confirm the role of endothelial Notch1 signaling in mediating CQ's effect on tumor vessel normalization in vivo, we analyzed the effect of CQ on tumor vessels in mice lacking *Notch1* in ECs (*Notch1*$^{EC\text{-}KO}$). These mice were generated by intercrossing *Notch1*$^{lox/lox}$ mice (Radtke et al., 1999) with *VE-cadherin(PAC)-Cre*^{ERT2} mice, an EC-specific inducible Cre-driver line (Benedito et al., 2012), and treating them with tamoxifen for 7 days. RT-PCR revealed decreased *Notch1* levels in ECs isolated from *Notch1*$^{EC\text{-}KO}$ mice (by 74 ± 5%; n = 5). Treatment of isogenic *Notch1*$^{EC\text{-}KO}$ mice with 50 mg/kg/day CQ did not affect B16-F10 tumor growth (Figure 8B). Notably, EC loss of *Notch1* completely abrogated the inhibitory effects of CQ on metastasis and tumor necrosis (Figures 8C and 8D).

EC-specific deficiency of *Notch1* itself already affected the tumor vasculature. Indeed, tumors from *Notch1*$^{EC\text{-}KO}$ mice were more hypoxic and formed more numerous, more tortuous, less mature, and hypoperfused vessels (Figures 8E–8J). Importantly, however, CQ treatment of *Notch1*$^{EC\text{-}KO}$ mice failed to reduce tumor vessel density, tortuosity, and tumor hypoxia and failed to increase vessel maturation and perfusion (Figures 8E–8J). These findings that endothelial loss of *Notch1* completely abrogated the inhibitory effects of CQ on tumor vessel normalization indicate that the vascular effects of CQ primarily relied on Notch1 signaling in vivo.

DISCUSSION

CQ is used as an autophagy blocker in anticancer treatment, but it is unknown if CQ exerts its effects solely by inhibiting autophagy in cancer cells. We identified an effect of CQ on tumor vessel normalization, which helps explain its antimetastatic and chemotherapy-enhancing actions.

Using two metastatic melanoma models, relying on heightened autophagy for their growth (Noman et al., 2011; Xie et al., 2013), we show that the anticancer activity of CQ is not only reliant on direct cancer cell killing through blockage of prosurvival autophagy (the sensitivity to this killing effect may vary between individual cancer cell types) but also or primarily relies on an effect on tumor vessels. Indeed, even at a dose that was ineffective to reduce tumor growth (50 mg/kg/day), CQ already modified the tumor milieu by improving tumor perfusion and oxygenation. Because metabolic stress stimulates autophagy, cancer cells growing in these CQ-treated tumors likely relied less on autophagy because they had access to more abundant oxygen and nutrients and were thus less sensitive to CQ's antiproliferative and cytotoxic activity.

CQ reduced tumor hypoxia, cancer cell invasion, intravasation, and spreading and improved the delivery and efficacy of chemotherapeutics. The better perfused, less chaotic, and tightened EC barrier in vivo observed after CQ treatment can explain the reduction in cancer cell intravasation and the number of circulating cancer cells (Mazzone et al., 2009). Moreover, because tumor hypoxia promotes metastasis (Carmeliet and Jain, 2011), CQ's effect on improving tumor oxygenation may contribute to the decreased cancer cell invasiveness and dissemination. Consistently, tumor vessel normalization often does not affect the size of primary tumors, but its benefit relates to reduction of metastasis and to the improved drug delivery and efficiency of chemotherapy (Carmeliet and Jain, 2011). A previous study reported that CQ is "vasculoprotective" (Hagihara et al., 2000) but did not assess vessel normalization. Further support that CQ's antimetastatic effects are likely mediated by cancer cell-nonautonomous mechanisms is provided by findings that CQ did not prevent colonization of cancer cells to the lungs after intravenous injection and invasion of cancer cells in vitro. Though CQ might have other antimetastatic effects that were not explored here, CQ at least partly prevented metastasis by promoting vessel normalization.

Unlike CQ, ATG5 knockdown in cancer cells did not improve tumor oxygenation and did not affect cancer cell invasion and intravasation but did increase tumor cell death. Except for the reduced tumor growth and metastasis, ATG5 knockdown overall did not phenocopy the effects of CQ on the tumor stroma. Regarding the mechanisms of metastasis, ATG5-silenced cancer cells also failed to colonize the lungs after intravenous injection, most likely because of their increased vulnerability to anoikis (Fung et al., 2008). In contrast, CQ reduced metastasis by impairing intravasation.

Blocking EC autophagy by ATG5 knockdown did also not phenocopy CQ-induced EC responses in vitro, nor did it affect tumor vessels in vivo. Although genetic loss of *Atg5* in ECs delayed tumor growth, it did not reduce the metastatic index and failed to evoke vessel normalization and improve tumor oxygenation. On the contrary, tumor vessels in *Atg5*$^{EC\text{-}KO}$ mice displayed smaller lumens and increased density and tortuosity and exhibited reduced vessel maturation and perfusion. Thus, genetic loss of autophagy in ECs exacerbated the chaotic and functionally abnormal tumor vasculature, while CQ produced the opposite effect. Overall, blockage of autophagy in ECs or cancer cells cannot explain CQ's ability to normalize tumor vessels.

Figure 7. Effect of CQ on Notch1 Signaling in ECs

(A) Immunoblotting for NICD, p120, and NEXT of ECs treated with CQ (25 μM) or DLL4 (0.5 μg/ml) for 12, 24, 48, or 72 hr (n = 3).

(B) Immunoblotting for NICD in nuclear and cytoplasmic extracts of ECs treated with CQ (25 μM) or DLL4 (0.5 μg/ml) for 24 hr. Loading control of the nuclear (lamin) and cytoplasmic (glyceraldehyde 3-phosphate dehydrogenase) fractions is shown. Densitometric quantification is shown below the lanes (n = 4).

(C) Immunostaining for NICD in ctrl- and CQ-treated cells (DAPI nuclear staining). Insets are magnifications of the boxed areas. Quantification of NICD^{+} area per nucleus is indicated. The scale bar represents 10 μm.

(D) RBPj dual luciferase reporter assay in ECs in response to CQ (25 μM) or DLL4 (0.5 μg/ml) after 12, 24, 48, or 72 hr (n = 3).

(E and F) RT-PCR analysis of the Notch target transcripts *HEY1* (E) and *HES1* (F) in ECs treated with CQ (25 μM) or DLL4 (0.5 μg/ml) for 12, 24, 48, or 72 hr (n = 6).

All quantitative data are mean ± SEM. *p < 0.05; **p < 0.01; ***p < 0.001. See also Figure S7.

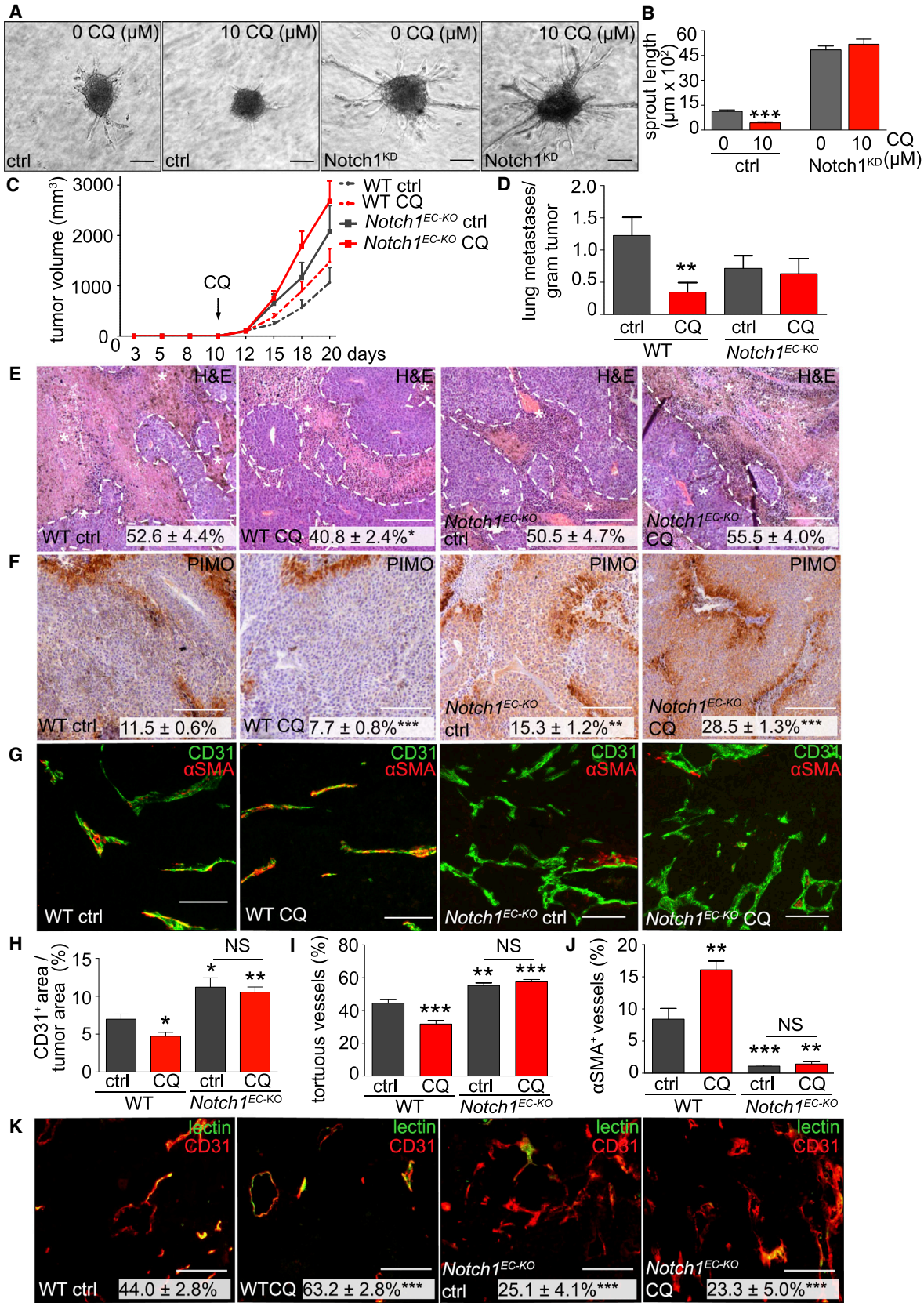

(legend on next page)

The vessel normalization effect of CQ phenocopied the vascular effects induced by Notch1 activation in tumor ECs, characterized by fewer but more perfused vessels, resulting in decreased intratumoral hypoxia (Li et al., 2007). In line, CQ normalized tumor vessels largely by increasing Notch1 signaling in ECs. Indeed, CQ reduced EC proliferation and migration and impaired vessel sprouting in vitro, known vascular effects of Notch (Phng and Gerhardt, 2009). CQ increased nuclear accumulation and the transcriptional activity of NICD, while Notch1 inhibition or knockdown abrogated CQ's effects in vitro. Our findings do not exclude the possibility that CQ can affect vessel normalization by regulating additional molecular pathways or by affecting other stromal cells. Importantly, however, all effects of CQ on tumor oxygenation, vessel normalization, tumor necrosis, and metastasis were completely reverted in mice lacking *Notch1* in ECs. These findings provide compelling evidence for an autophagy-independent and Notch1-requiring mechanism of CQ to promote normalization of the tumor vasculature.

How then does CQ increase Notch1 signaling in ECs? Processing of Notch1 to NICD by γ-secretase can occur at different sites, from the plasma membrane up to endosomal compartments. Notably, CQ induced a prominent accumulation of Notch1 in LEs and lysosomes, degradative compartments that are important signaling hubs, a process that did not require activation of Notch1 by its ligands. Different experimental approaches support the following model: CQ has no effect on cell surface-localized shedding of p120 by ADAMs and thus does not affect p120 levels. Instead, by compromising LE and lysosomal function (through alkalinization) and reducing lysosomal degradation, CQ induces an accumulation of NEXT, thereby providing a larger source of this substrate for γ-secretase, which thus can generate higher amounts of NICD. This results in sustained activation of Notch1 signaling, sufficient to induce tumor vessel normalization.

Activation of Notch1 signaling by CQ is different from that induced by DLL4. In this case, ligand binding induces shedding of p120 by ADAMs to produce NEXT. Because LE and lysosomal functions are normal, further proteolysis by γ-secretase can keep pace with the increased production of NEXT, preventing its accumulation and leading to a more transient increase in NICD and Notch1 signaling.

Tumor vessel normalization improves the delivery and efficacy of chemotherapy (Carmeliet and Jain, 2011). We show a greater tumor-inhibitory effect when CQ is combined with chemotherapy. Because CQ did not sensitize tumor cells to CPt in vitro but only in vivo, CQ's effect on the chemoresponse is likely due to its cancer cell-extrinsic vessel normalization effects, which increase the delivery of cytotoxic agents to the tumor core because of improved perfusion. Vessel normalization also reduces the interstitial fluid pressure in tumors, thereby facilitating egress of cytotoxic agents from the blood into the tumor interstitium (Leite de Oliveira et al., 2012). Also, because the efficacy of cytotoxic agents relies on oxygenation to generate oxygen radicals, CQ improved the chemotherapy response by reducing tumor hypoxia as well. Consistently, CQ enhanced the anticancer effect of radiotherapy and lowered tumor hypoxia (Rouschop et al., 2010). Although the mechanisms were not studied in this report, on the basis of our results, the improved tumor oxygenation might have been due to CQ-mediated vessel normalization. Vessel normalization also facilitates the access of immune cells to tumors and converts the immunosuppressive into an immunostimulatory milieu (Huang et al., 2012). Noteworthy, CQ potentiates antitumor responses induced by vaccination or immune cell infiltration (Liang et al., 2012; Noman et al., 2011). It will be interesting to explore if CQ, besides its immunodampening effects (Townsend et al., 2012), can regulate tumor immunity via effects on vessel normalization.

A recent survey on the use of CQ and hydrochloroquine as mainstay treatments for autoimmune pathologies commented that these antimalarial drugs also exert vasculoprotective, antithrombotic, and possibly even antineoplastic effects, while warning caution against rare retinal toxicity events (Lee et al., 2011). The property of CQ as a clinically approved drug to induce persistent tumor vessel normalization makes this agent especially attractive for anticancer therapy.

EXPERIMENTAL PROCEDURES

Detailed methods are described in Supplemental Experimental Procedures.

Cell Culture and In Vitro Functional Assays

Human umbilical vein ECs (HUVECs) and cancer cells were cultured as described in Supplemental Experimental Procedures. Autophagic flux detection was determined via immunoblotting for LC3 and p62 or immunostaining of LC3. Cell death was analyzed by propidium iodide (PI) exclusion and quantified by flow cytometry. Proliferation was quantified by measuring [^{3}H]-thymidine incorporation. To assess clonogenic growth, the number of colonies formed by single cells was analyzed after 7 days. EC spheroids were embedded in collagen gel and cultured for 24 hr to induce sprouting.

Figure 8. Effect of Genetic Deficiency of *Notch1* in ECs on CQ Phenotypes

(A and B) Representative micrographs (A) and quantification of sprout length (B) (n = 20) of spheroids of Notch1-silenced (Notch1^{KD}) ECs compared with control scrambled shRNA-treated ECs (ctrl) in the presence or absence of CQ.

(C) Growth curve of B16-F10 tumors in WT mice and in *Notch1*$^{EC-KO}$ mice treated with CQ (50 mg/kg/day) or PBS (n = 12–14).

(D) Metastatic index in B16-F10 tumor-bearing WT and *Notch1*$^{EC-KO}$ mice treated with or without CQ (n = 41–54).

(E) Micrographs of H&E staining of necrotic areas (asterisks within dashed lines) in B16-F10 tumors in WT versus *Notch1*$^{EC-KO}$ treated with CQ or vehicle. Quantification of necrotic tumor area is indicated (percentage of total; n = 4–6).

(F) Micrographs of PIMO staining of hypoxic zones in B16-F10 tumors from WT and *Notch1*$^{EC-KO}$ mice treated with vehicle or CQ. Quantification is indicated percentage of total; (n = 5–9).

(G–J) Immunostaining for CD31 and αSMA of B16-F10 tumors from WT and *Notch1*$^{EC-KO}$ mice, treated with vehicle or CQ (G) and quantification of CD31$^+$ tumor vessel area expressed as percentage of the total area (H), percentage of tortuous vessels (I), and percentage of pericyte-covered vessels (J) (n = 4).

(K) Micrographs of lectin-FITC-perfused and CD31-stained vessels in B16-F10 tumors in WT and *Notch1*$^{EC-KO}$ mice treated with vehicle or CQ. Quantification of perfusion (CD31$^+$lectin$^+$ area, percentage of total CD31$^+$ area) is included (n = 3).

Scale bars represent 200 μm (A, E, and F) and 100 μm (G and K). All data are mean ± SEM. *p < 0.05; **p < 0.01; ***p < 0.001. Significance for all conditions is quantified relative to WT ctrl, unless indicated with the bar. See also Figure S8.

Number and sprout length were analyzed with Image J software (NIH). A scratch wound was applied on confluent EC monolayers in 24-wells after overnight CQ pretreatment. Migration distance was measured with Image J software. Cancer cells were seeded on Matrigel, and invasion was quantified after 48 hr by measuring the area of cancer cell invasion into Matrigel.

Treatments

CQ- or shRNA-mediated human ATG5 or murine ATG5 targeting were used to inhibit autophagy. For Notch pathway activation, cells were grown on plates coated with recombinant human DLL4 extracellular domain. Inhibition of Notch activity was achieved by culturing cells in the presence of 10 μM DAPT or by shRNA-mediated Notch1,2,3,4 silencing. Baf and Dynasore were used to block the vacuolar H^+ ATPase and internalization, respectively.

RT-PCR, Immunoblotting, and Immunocytochemistry

mRNA expression was analyzed by quantitative RT-PCR. Immunoblotting and immunostaining were performed using methods and antibodies listed in Supplemental Experimental Procedures.

Mouse Models

Animal procedures were approved by the Institutional Animal Care and Research Advisory Committee (KU Leuven) (ECD118/2013) and were performed in accordance with the institutional and national guidelines and regulations. To assess subcutaneous tumor growth, 150,000 B16-F10 (murine) or 300,000 A375m (human) melanoma cells were injected subcutaneously into the right flanks of immunocompetent syngeneic (C57/Bl6) or immunodeficient (nu/nu) mice, respectively. Tumor volumes were measured three times per week with a caliper using the formula $V = \pi \times [d^2 \times D]/6$, where d is the minor tumor axis and D is the major tumor axis. For experimental metastasis, 200,000 B16-F10 cells were injected in the tail veins of C57/Bl6 mice, and after 14 days, mice were sacrificed and lungs collected.

Patient Samples

Biopsies from melanoma and healthy skin were collected at the university hospital of Leuven with patients' informed consent, in accordance with the Declaration of Helsinki and with the approval of the Medical Ethics Committee of the university hospital.

Statistics

Data displayed in the figures and text represent mean ± SEM of representative experiments unless otherwise stated; each experiment was repeated at least three times and involved at least triplicate measurements. Statistical significance was calculated by standard t test or ANOVA. A p value < 0.05 was considered significant.

SUPPLEMENTAL INFORMATION

Supplemental Information includes Supplemental Experimental Procedures and eight figures and can be found with this article online at http://dx.doi.org/10.1016/j.ccr.2014.06.025.

ACKNOWLEDGMENTS

We acknowledge S. Van Eygen, K. Rillaerts, L. Notebaert, V. Baert, L. Serneels, H. Acx, L. Chavez-Guiterez, and VRC core facilities; B. Floot for providing NKI-A59; J. van den Oord for providing biopsies; and P. Boya for *Atg5*$^{lox/lox}$ mice. Supporting fellowships: K.D.B., A.K., A.Q., and A.P.: FWO; S.S., S.M., and J.W.: VLK; S.S. and H.M.: IWT. Supporting grants: P.C.: IUAP P7/03 (Belgian Science Policy), Methusalem funding, GOA2006/11 (also to M.D.), FWO G.0598.12, G.0692.09, G.0532.10, G.0817.11, 1.5.202.10.N Krediet aan navorsers, the Foundation Leducq Transatlantic Network (ARTEMIS) and ERC Advanced Research Grant (EU-ERC269073); E.D.: ERC Advanced Research Grant (EU-ERC268870); P.A.: FWO G.0661.09, G.0728.10, G.0584.12N, IUAP7/32 (Belgian Science Policy), and KU Leuven GOA/11/009 (also to W.A.).

Received: December 19, 2012
Revised: January 6, 2014
Accepted: June 27, 2014
Published: August 11, 2014

REFERENCES

Andersson, E.R., Sandberg, R., and Lendahl, U. (2011). Notch signaling: simplicity in design, versatility in function. Development *138*, 3593–3612.

Baron, M. (2012). Endocytic routes to Notch activation. Semin. Cell Dev. Biol. *23*, 437–442.

Benedito, R., Rocha, S.F., Woeste, M., Zamykal, M., Radtke, F., Casanovas, O., Duarte, A., Pytowski, B., and Adams, R.H. (2012). Notch-dependent VEGFR3 upregulation allows angiogenesis without VEGF-VEGFR2 signalling. Nature *484*, 110–114.

Carmeliet, P., and Jain, R.K. (2011). Principles and mechanisms of vessel normalization for cancer and other angiogenic diseases. Nat. Rev. Drug Discov. *10*, 417–427.

De Strooper, B., and Annaert, W. (2010). Novel research horizons for presenilins and γ-secretases in cell biology and disease. Annu. Rev. Cell Dev. Biol. *26*, 235–260.

Dill, M.T., Rothweiler, S., Djonov, V., Hlushchuk, R., Tornillo, L., Terracciano, L., Meili-Butz, S., Radtke, F., Heim, M.H., and Semela, D. (2012). Disruption of Notch1 induces vascular remodeling, intussusceptive angiogenesis, and angiosarcomas in livers of mice. Gastroenterology *142*, 967–977, e2.

Eichmann, A., and Simons, M. (2012). VEGF signaling inside vascular endothelial cells and beyond. Curr. Opin. Cell Biol. *24*, 188–193.

Fortini, M.E. (2009). Notch signaling: the core pathway and its posttranslational regulation. Dev. Cell *16*, 633–647.

Fung, C., Lock, R., Gao, S., Salas, E., and Debnath, J. (2008). Induction of autophagy during extracellular matrix detachment promotes cell survival. Mol. Biol. Cell *19*, 797–806.

Guarani, V., Deflorian, G., Franco, C.A., Krüger, M., Phng, L.K., Bentley, K., Toussaint, L., Dequiedt, F., Mostoslavsky, R., Schmidt, M.H., et al. (2011). Acetylation-dependent regulation of endothelial Notch signalling by the SIRT1 deacetylase. Nature *473*, 234–238.

Hagihara, N., Walbridge, S., Olson, A.W., Oldfield, E.H., and Youle, R.J. (2000). Vascular protection by chloroquine during brain tumor therapy with Tf-CRM107. Cancer Res. *60*, 230–234.

Hara, T., Nakamura, K., Matsui, M., Yamamoto, A., Nakahara, Y., Suzuki-Migishima, R., Yokoyama, M., Mishima, K., Saito, I., Okano, H., and Mizushima, N. (2006). Suppression of basal autophagy in neural cells causes neurodegenerative disease in mice. Nature *441*, 885–889.

Harrington, L.S., Sainson, R.C., Williams, C.K., Taylor, J.M., Shi, W., Li, J.L., and Harris, A.L. (2008). Regulation of multiple angiogenic pathways by Dll4 and Notch in human umbilical vein endothelial cells. Microvasc. Res. *75*, 144–154.

Huang, Y., Yuan, J., Righi, E., Kamoun, W.S., Ancukiewicz, M., Nezivar, J., Santosuosso, M., Martin, J.D., Martin, M.R., Vianello, F., et al. (2012). Vascular normalizing doses of antiangiogenic treatment reprogram the immunosuppressive tumor microenvironment and enhance immunotherapy. Proc. Natl. Acad. Sci. U S A *109*, 17561–17566.

Lee, S.J., Silverman, E., and Bargman, J.M. (2011). The role of antimalarial agents in the treatment of SLE and lupus nephritis. Nat. Rev. Nephrol. *7*, 718–729.

Leite de Oliveira, R., Deschoemaeker, S., Henze, A.T., Debackere, K., Finisguerra, V., Takeda, Y., Roncal, C., Dettori, D., Tack, E., Jönsson, Y., et al. (2012). Gene-targeting of Phd2 improves tumor response to chemotherapy and prevents side-toxicity. Cancer Cell *22*, 263–277.

Li, J.L., Sainson, R.C., Shi, W., Leek, R., Harrington, L.S., Preusser, M., Biswas, S., Turley, H., Heikamp, E., Hainfellner, J.A., and Harris, A.L. (2007). Delta-like 4 Notch ligand regulates tumor angiogenesis, improves tumor vascular function, and promotes tumor growth in vivo. Cancer Res. *67*, 11244–11253.

Liang, X., De Vera, M.E., Buchser, W.J., Romo de Vivar Chavez, A., Loughran, P., Beer Stolz, D., Basse, P., Wang, T., Van Houten, B., Zeh, H.J., 3rd, and Lotze, M.T. (2012). Inhibiting systemic autophagy during interleukin 2 immunotherapy promotes long-term tumor regression. Cancer Res. *72*, 2791–2801.

Liu, Z., Turkoz, A., Jackson, E.N., Corbo, J.C., Engelbach, J.A., Garbow, J.R., Piwnica-Worms, D.R., and Kopan, R. (2011). Notch1 loss of heterozygosity causes vascular tumors and lethal hemorrhage in mice. J. Clin. Invest. *121*, 800–808.

Maes, H., Rubio, N., Garg, A.D., and Agostinis, P. (2013). Autophagy: shaping the tumor microenvironment and therapeutic response. Trends Mol. Med. *19*, 428–446.

Mazzone, M., Dettori, D., Leite de Oliveira, R., Loges, S., Schmidt, T., Jonckx, B., Tian, Y.M., Lanahan, A.A., Pollard, P., Ruiz de Almodovar, C., et al. (2009). Heterozygous deficiency of PHD2 restores tumor oxygenation and inhibits metastasis via endothelial normalization. Cell *136*, 839–851.

Mizushima, N., Levine, B., Cuervo, A.M., and Klionsky, D.J. (2008). Autophagy fights disease through cellular self-digestion. Nature *451*, 1069–1075.

Müller, C.S. (2012). Notch signaling and malignant melanoma. Adv. Exp. Med. Biol. *727*, 258–264.

Noman, M.Z., Janji, B., Kaminska, B., Van Moer, K., Pierson, S., Przanowski, P., Buart, S., Berchem, G., Romero, P., Mami-Chouaib, F., and Chouaib, S. (2011). Blocking hypoxia-induced autophagy in tumors restores cytotoxic T-cell activity and promotes regression. Cancer Res. *71*, 5976–5986.

Oberlin, E., El Hafny, B., Petit-Cocault, L., and Souyri, M. (2010). Definitive human and mouse hematopoiesis originates from the embryonic endothelium: a new class of HSCs based on VE-cadherin expression. Int. J. Dev. Biol. *54*, 1165–1173.

Peng, Y.F., Shi, Y.H., Ding, Z.B., Ke, A.W., Gu, C.Y., Hui, B., Zhou, J., Qiu, S.J., Dai, Z., and Fan, J. (2013). Autophagy inhibition suppresses pulmonary metastasis of HCC in mice via impairing anoikis resistance and colonization of HCC cells. Autophagy *9*, 2056–2068.

Phng, L.K., and Gerhardt, H. (2009). Angiogenesis: a team effort coordinated by notch. Dev. Cell *16*, 196–208.

Radtke, F., Wilson, A., Stark, G., Bauer, M., van Meerwijk, J., MacDonald, H.R., and Aguet, M. (1999). Deficient T cell fate specification in mice with an induced inactivation of Notch1. Immunity *10*, 547–558.

Rouschop, K.M., van den Beucken, T., Dubois, L., Niessen, H., Bussink, J., Savelkouls, K., Keulers, T., Mujcic, H., Landuyt, W., Voncken, J.W., et al. (2010). The unfolded protein response protects human tumor cells during hypoxia through regulation of the autophagy genes MAP1LC3B and ATG5. J. Clin. Invest. *120*, 127–141.

Sannerud, R., and Annaert, W. (2009). Trafficking, a key player in regulated intramembrane proteolysis. Semin. Cell Dev. Biol. *20*, 183–190.

Townsend, K.N., Hughson, L.R., Schlie, K., Poon, V.I., Westerback, A., and Lum, J.J. (2012). Autophagy inhibition in cancer therapy: metabolic considerations for antitumor immunity. Immunol. Rev. *249*, 176–194.

White, E. (2012). Deconvoluting the context-dependent role for autophagy in cancer. Nat. Rev. Cancer *12*, 401–410.

Xie, X., White, E.P., and Mehnert, J.M. (2013). Coordinate autophagy and mTOR pathway inhibition enhances cell death in melanoma. PLoS ONE *8*, e55096.

Yan, M., Callahan, C.A., Beyer, J.C., Allamneni, K.P., Zhang, G., Ridgway, J.B., Niessen, K., and Plowman, G.D. (2010). Chronic DLL4 blockade induces vascular neoplasms. Nature *463*, E6–E7.

Zhang, J., Fukuhara, S., Sako, K., Takenouchi, T., Kitani, H., Kume, T., Koh, G.Y., and Mochizuki, N. (2011). Angiopoietin-1/Tie2 signal augments basal Notch signal controlling vascular quiescence by inducing delta-like 4 expression through AKT-mediated activation of beta-catenin. J. Biol. Chem. *286*, 8055–8066.